



ORIGINAL ARTICLE

Cell-selective titanium oxide coatings mediated by coupling hafnium-doping and UV pre-illumination

Peishi Wu^{a,b}, Huiliang Cao^{b,*}, Jinshu Guo^b, Qiming Luo^b, Yuanyuan Cui^{a,*},
Xuanyong Liu^{b,*}

^a School of Materials Science and Engineering, Shanghai University, Shanghai 200444, China

^b State Key Laboratory of High Performance Ceramics and Superfine Microstructure, Shanghai Institute of Ceramics, Chinese Academy of Sciences, 200050, China

Received 20 February 2019; accepted 2 July 2019

Available online 9 July 2019

KEYWORDS

Titanium;
Surface modification;
Ultraviolet;
Bacteria;
Hafnium

Abstract Cell-selective biomaterials, i.e. favoring the functions of gingival cells and simultaneously reducing the adhesion of pathogenic bacteria, is highly desired in dental implants. However, due to the same mechanisms shared in attachment by mammalian and microbial cells, it is hard to increase the functions of the former while acting against the latter. Herein, a cell-selectivity was established on titanium oxide coatings by combining a plasma immersion ion implantation & deposition (PIII) and a UV pre-illumination. The titanium oxide coatings were produced on pure titanium substrates by using a plasma electrolytic oxidation technique and then doped of hafnium (Hf) by using a cathodic arc sourced PIII. The Hf-doped titanium oxide coatings (Hf-PIII groups) were capable of delaying the recombination of UV-illumination generated electron-hole pairs, which decreased the adhesion of bacterial cells at the later period (cultured for 24 h). Titanium oxide coating doped of 4.87 at.% hafnium (Hf) gained the biggest decrease (decreased 52.9% compared to its UV negative counterparts) in bacterial adhesion among the UV positive (UV⁺) groups. This study demonstrates that coupling Hf-doping and UV pre-illumination is promising for improving the cell-selective performance of titanium-based dental implants.

© 2019 Production and hosting by Elsevier B.V. on behalf of King Saud University. This is an open access article under the CC BY-NC-ND license (<http://creativecommons.org/licenses/by-nc-nd/4.0/>).

1. Introduction

Titanium-based materials are commonly used as dental implants because of their excellent biocompatibility and corrosion resistance property (Ananth et al., 2015); however, these materials are facing the challenge of bacterial adhesion, which is an answer for the premature failure of a large number of oral implants annually (Renvert et al., 2018). It was reported that peri-implantitis affects about 28% to 56% of implant-carrying patients, which is a key factor undermining

* Corresponding authors.

E-mail addresses: hlc@mail.sic.ac.cn (H. Cao), cui-yy@shu.edu.cn (Y. Cui), xyliu@mail.sic.ac.cn (X. Liu).

Peer review under responsibility of King Saud University.



Production and hosting by Elsevier

the stability and lifespan of the implants (Derks and Tomasi, 2015). Peri-implant mucositis (soft tissue infection surrounding a dental implant) is the precursory step leading to peri-implantitis, and a good biological sealing decreases the risk of peri-implantitis (Zhang et al., 2018). Accordingly, making biomaterials cell-selective, for example favoring the functions of gingival cells and simultaneously reducing the adhesion of pathogenic bacteria, is highly desired in clinical applications (Cao et al., 2018; Gristina, 1987; Sanz-Martin et al., 2018).

It is believed that the excellent biocompatibility of titanium-based materials stems from the spontaneously formed titanium oxide layer (Williams, 2008), which can be activated by light illumination (Miyachi et al., 2010), becoming more hydrophilic that subsequently contribute to improved mammalian-cell adhesion and tissue integration (Areid et al., 2018; Iwasa et al., 2010; Miyachi et al., 2010; Yadav et al., 2017). And it was also demonstrated that light illumination could help titanium oxide decomposing the adherent pathogenic microbes and viruses via separating the electron-hole pairs on the materials (Nakano et al., 2012; Visai et al., 2011). Since mammalian cells and bacteria share many of the same mechanisms in the attachment (Busscher et al., 2012), it is still unclear whether a UV treatment can increase the attachment of the former while simultaneously decreasing the adhesion of the latter. In addition, most of the previous studies were focusing on activating the antibacterial actions of titanium oxide by a light-irradiation *in situ* bacterial culture (Fujishima et al., 2008), which may possibly induce serious mutations in mammalian cells (Glazer et al., 1986), undermining the establishment of cell-selectivity. Previously, a post-irradiation activity against bacterial adhesion was found on Ti6Al4V and pure titanium surfaces (de Avila et al., 2015; Gallardo-Moreno et al., 2010), which could spontaneously be covered by a thin titanium oxide layer while exposing to the atmosphere (Cao and Liu, 2013). However, this efficacy of post-illumination could be lost within a very short time (about 60 min) after UV-irradiation (Gallardo-Moreno et al., 2010), which is hard to be applied in clinic treatments. Improving charge separation by metal doping is believed to be an effective way to modify the light responsive behaviors of titanium oxide (Cao and Liu, 2013), which possibly improves the post-irradiation activity of the material. Although the coupling of hafnium (Hf) was found effective in enhancing the light sensitivity of titanium oxide (Cadieu and Murokh, 2017), the effect of Hf-doping on the cell-selectivity of the material is still enigmatic.

Accordingly, the aim of this study is to fabricate hafnium (Hf)-doped titanium oxide coating and evaluate its effects on the adhesion of bacterial cells and gingival fibroblasts. Interestingly, the Hf-doped titanium oxide coatings had a delayed electron-hole recombination behavior, which likely facilitated the storage of the charge generated during UV pre-illumination, and hence the establishment of a cell-selectivity on the materials.

2. Materials and methods

2.1. Preparation of the coatings

Titanium oxide (denoted as TO) was coated on the commercial pure titanium plates (10 mm squares with a thickness of 1 mm, Grade 2) by carrying out plasma electrolytic oxidation in a

solution of glycerophosphate disodium salt pentahydrate (8.0 g/L, Kelong, China) and sodium metasilicate nonahydrate (8.0 g/L, Sinopharm, China). Then, the TO coatings were further treated by hafnium (Hf) cathodic arc sourced plasma immersion ion implantation & deposition (Hf-PIII) at a bias potential of 30KV for 30, 60 and 90 min (denoted as TO-Hf30, TO-Hf60, and TO-Hf90, respectively). In order to study the post effects of light-illumination, the coatings were further exposed to an ultraviolet (UV) lamps for 24 h (UV positive groups, UV⁺). The UV lamps emitted light at a wavelength of 365 nm (Cnlight, China). The samples were positioned about 8 cm away from the lamps, receiving a UV intensity of about 30 mW/cm².

2.2. Material characterization

The surface morphologies of the coatings were examined by scanning electron microscopy (SEM; JEOLJSM-6700F, Japan). The composition and chemical states of the concerned compositions were determined by X-ray photoelectron spectroscopy (XPS) (Physical electronics PHI 5802). The phase structure of the samples was detected using X-ray diffractometer (D2 PHASER, Bruker, Germany) with a Cu K α X-ray source, data sets were collected over the range of 5°-80°, with a step size of 0.02° (2 θ) and a count rate of 5°/min. Dynamic potential polarization curves were acquired from the samples in a physiological saline solution (0.9% NaCl at pH of 7) using an AUTOLAB electrochemical workstation (Switzerland). The measurement was conducted using a conventional three-electrode system, i.e. a saturated calomel electrode (SCE) was served as the reference electrode, a graphite rod was served as the counter electrode, and the sample with a 0.3 cm² area exposed was served as the working electrode. Prior to the polarization test, the samples were stabilized in the solution for 30 min and the tests were conducted at room temperature at a scanning rate of 60 mV/min. The photoluminescence (PL) spectra of the coatings before and after UVA illumination were recorded via a Fluoromax-4 spectrometer by using an excitation wavelength of 300 nm. The wettability of the sample surfaces with and without a UVA treatment was evaluated by using an automated contact angle measuring device (SL200B, Solon, China) and a 1 μ L of pure water.

2.3. Adhesion of bacterial cells

The adhesion of *Staphylococcus aureus* (*S. aureus*, ATCC 25923) on the coatings was evaluated by SEM. The samples without UV treatment were sterilized at room temperature with 75% ethanol and replaced once every half hour for 4 consecutive times. Then, a 60 μ L of bacterial suspension at a concentration of 10⁷ CFU/mL was introduced onto each sample immediately after the alcohol (dried) or UV treatments. After incubating at 37 °C for 6 h or 24 h in the dark, the bacterial cells were fixed with 2.5% glutaraldehyde solution and dehydrated as we described previously (Cao et al., 2013, 2014). The samples were subsequently subjected to SEM observations. The number (N) of the adherent bacterial cells on each group was counted by using the SEM images, and the bacterial density (BD) for the samples were calculated by dividing the area (S) of the corresponding SEM image, i.e. BD = N/S. Three locations of each group were estimated to obtain a statistical result.

2.4. Adhesion of mammalian cells

The adhesion of mammalian cells was evaluated by using the human gingival fibroblasts (HGF) (Stem Cell Bank, Chinese Academy of Sciences, Shanghai, China). The cells in a density of 2×10^4 cells/mL were introduced on the coatings and cultured at 37°C in 24-well culture plates. Every well contained 1 mL of DMEMF-12 supplemented with 10% fetal bovine serum (FBS) (Hyclone, USA) and 1% antimicrobial of penicillin and streptomycin (Antibiotic-Antimycotic, Hyclone, USA). After culturing for 1 h and 3 h, the cells were rinsed twice by phosphate buffer saline (PBS), fixed with 4% paraformaldehyde (PFA) solution at room temperature, and stained with FITC-Phalloidin and DAPI. The F-actin and cell nuclei were examined on fluorescence microscopy (Olympus, Japan). The areas of the spreading cells and the corresponding fluorescent image was measured respectively by using Image J, and then the ratio of the two areas was calculated. Three locations of each sample group were estimated.

2.5. Statistical analysis

Statistically significant differences between the sample groups were measured by an analysis of variance. All the analysis was carried out by using a GraphPad Prism 5 statistical software package. The data were reported as the mean and standard deviation (SD).

3. Results

3.1. Surface characteristics of the coatings

Fig. 1 shows the surface morphologies of the plasma electrolytically produced titanium oxide (TO) coatings before and after Hf-PIII treatments at 30 kV for 30, 60 and 90 min (denoted as TO-Hf30, TO-Hf60, and TO-Hf90, respectively). Incorporation of Hf did not alter the porous morphology of the TO coatings; however, some small cracks were detected around the pores (as shown by the insert in Fig. 1a) on the TO samples, and they healed as the Hf-PIII duration increases and disappeared eventually on the TO-Hf90 group (as shown by the inserts in Fig. 1b, c, and d). The phase structure of the TO

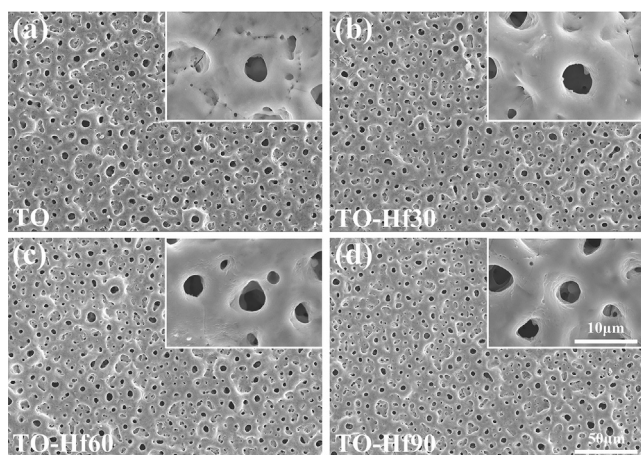


Fig. 1 SEM surface morphology of the samples: (a) the TO, (b) TO-Hf30, (c) TO-Hf60, (d) TO-Hf90.

and Hf-PIII treated groups was examined by X-ray diffraction (XRD). No significant difference to the peak positions was recorded in the XRD spectra (Fig. 2), all of the coatings had the basic phase structure (compose of anatase and rutile). The concentration and the chemical states of the doped Hf were evaluated by X-ray photoelectron spectroscopy (XPS). As shown by the XPS surveys (Fig. 3a), the intensity of the

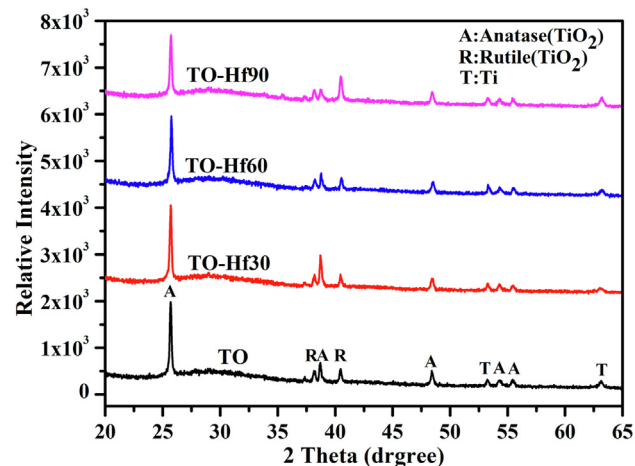


Fig. 2 X-ray diffraction spectra of the TO and Hf-doped titanium oxide coatings.

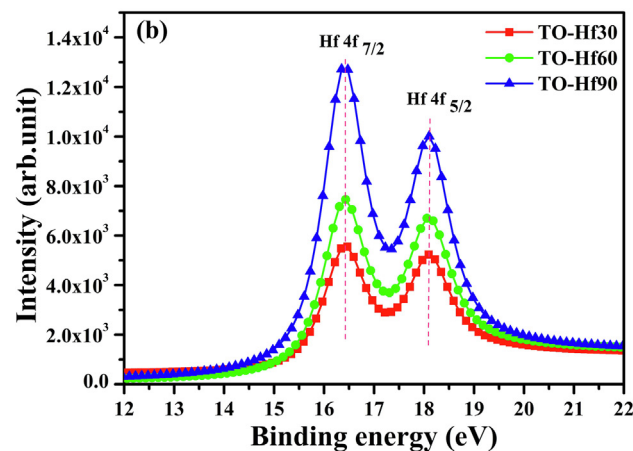
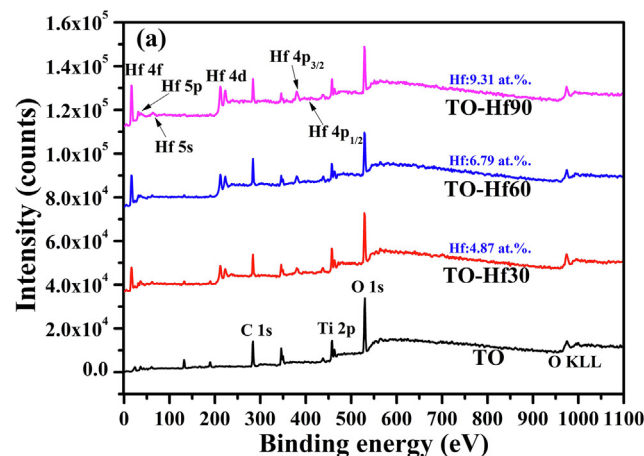


Fig. 3 XPS spectra of the samples: (a) the surveys, (b) the high-resolution spectra of Hf 4f.

Hf peaks increases as the Hf-PIII duration prolonged from 30 to 90 min, which was consistent with the change of hafnium concentration for the TO-Hf30, TO-Hf60, and TO-Hf90 groups, i.e. 4.87 at.%, 6.79 at.%, and 9.31 at.%, respectively. No apparent energy shift of Hf 4f (showed by the high-resolution spectra, Fig. 3b) among the Hf-PIII groups was detected. The Hf 4f doublet at 18.1 eV and 16.4 eV (with a separation of 1.7 eV) is corresponding to the HfO₂ (Domaradzki et al., 2006, Wang et al., 2004).

In order to evaluate the corrosion resistance of the samples, dynamic potential polarization tests were carried out in a 0.9% NaCl solution. The corrosion potentials acquired from the Hf-PIII groups shift positively compared to the TO control, from about -0.46 V for the TO-Hf30 group to about -0.14 V for the TO-Hf90 group (Fig. 4). Moreover, the corresponding polarization resistance of the TO-Hf30, TO-Hf60, and TO-Hf90 groups was $1.61 \times 10^6 \Omega\text{-cm}^2$, $3.18 \times 10^6 \Omega\text{-cm}^2$, and $4.30 \times 10^8 \Omega\text{-cm}^2$, respectively, which was 0.99, 1.95, and 264 times that of the TO group (see Table 1).

It was reported that the light sensitivity of hafnium doped titanium oxide was arisen by the oxygen-depleted regions in the composite (Cadieu and Murokh, 2017). Since the concentration of oxygen vacancies in a material is highly correlated to its photoluminescence (PL) signals (Chuang et al., 2012), the coatings were further studied by using PL spectra. The results demonstrated that Hf-PIII treatment apparently decreased the PL signals of TO (Fig. 5), indicating that Hf-doping was capable of delaying the recombination of photoinduced electron-hole pairs formed during light illumination. Moreover, the TO-Hf30 with small hafnium (Hf) concentra-

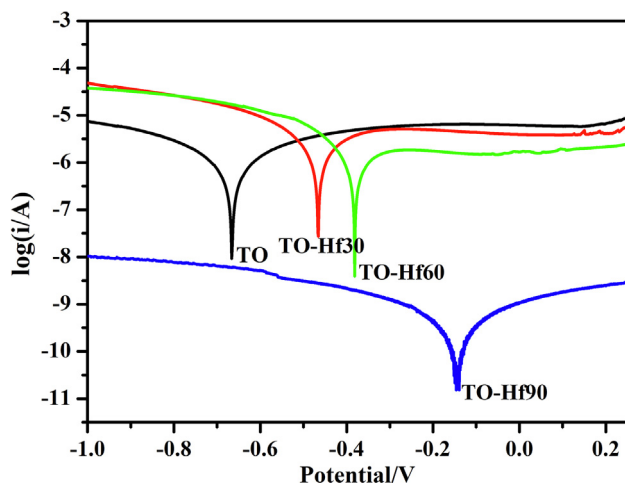


Fig. 4 Dynamic potential polarization curves of the samples.

Table 1 Parameters for the polarization curves.

Samples	Corrosion potential (V)	Corrosion current (A/cm ²)	Polarization resistance (Ω·cm ²)
TO	0.66	4.06×10^{-7}	1.63×10^6
TO-Hf30	0.46	2.86×10^{-7}	1.61×10^6
TO-Hf60	0.38	1.19×10^{-7}	3.18×10^6
TO-Hf90	0.14	3.25×10^{-10}	4.30×10^8

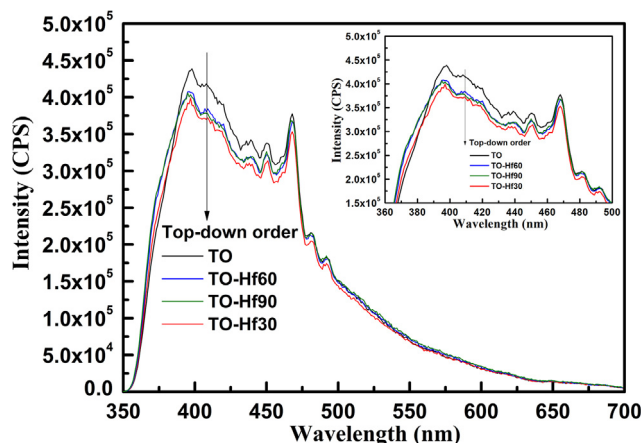


Fig. 5 Photoluminescence (PL) spectra of the TO and Hf-doped titanium oxide coatings, obtained by using an excitation wavelength of 300 nm.

tion (4.87 at.%) gained the biggest PL signal decrease compared to the other Hf-doped groups with big Hf concentrations, suggesting that the light sensitivity of the composite could be undermined by overdose Hf.

The wettability of the samples was determined by testing the water contact angles. As shown in Fig. 6, before UV illumination (the UV negative groups), the contact angle of the TO, TO-Hf30, TO-Hf60, and TO-Hf90 groups was 91.46°, 102.56°, 107.64°, and 110.92° respectively; however, after UV illumination, the corresponding contact angle was reduced to 58.81°, 75.89°, 82.40°, and 85.48°.

3.2. Adhesion of bacterial cells

The adhesion of the bacterial cells was evaluated by introducing *S. aureus* onto the samples and incubating for 6 h or 24 h. The surface morphology of the adherent microbes was examined by SEM. The bacterial cells on all the sample groups were normal without apparent distortion and any cytosolic content leakage

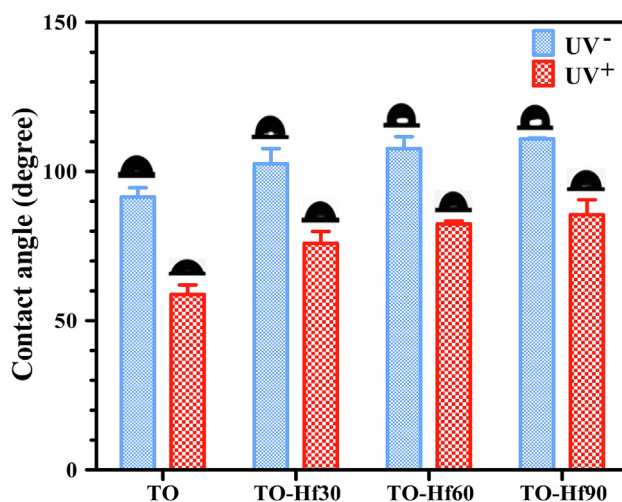


Fig. 6 Contact angles of the samples with (UV⁺) or without (UV⁻) UV pre-irradiation.

(Figs. 7 and 8), indicating that Hf-doping and UV illumination did not dramatically affect the viability of adherent bacteria. However, the amounts of bacterial cells were remarkably different among the groups. As for incubation of 6 h (Fig. 9a), the average bacterial density (BD) for TO, TO-Hf30, TO-Hf60, and TO-Hf90 was 6.25×10^6 cell/cm², 1.09×10^7 cell/cm², 1.10×10^7 cell/cm², and 1.63×10^7 cell/cm², respectively. And the BD values for those UV pre-treated groups were all increased to about 2.10×10^7 cell/cm², 1.76×10^7 cell/cm², 1.92×10^7 cell/cm², and 2.20×10^7 cell/cm², respectively. This result demonstrated that both Hf-doping and UV pre-illumination improved the initial adhesion of bacterial cells on titanium oxide. As for culturing of 24 h, the BD values for the TO, TO-Hf30, TO-Hf60, and TO-Hf90 groups (UV⁻ groups) were 5.99×10^7 cell/cm², 3.10×10^8 cell/cm², 2.33×10^8 cell/cm², and 2.33×10^8 cell/cm², respectively. And those for the corresponding UV positive (UV⁺) groups were 1.64×10^8 cell/cm², 1.46×10^8 cell/cm², 1.56×10^8 cell/cm², and 1.65×10^8 cell/cm², respectively. The BD values for all the UV positive Hf-PIII were decreased compared to their counterpart (the TO-Hf30 gained the biggest decrease among the Hf-doped groups, i.e. 52.9%), whereas the UV positive TO group gained an increase (increased 173.7%) compared to its UV negative counterpart. These results demonstrated that

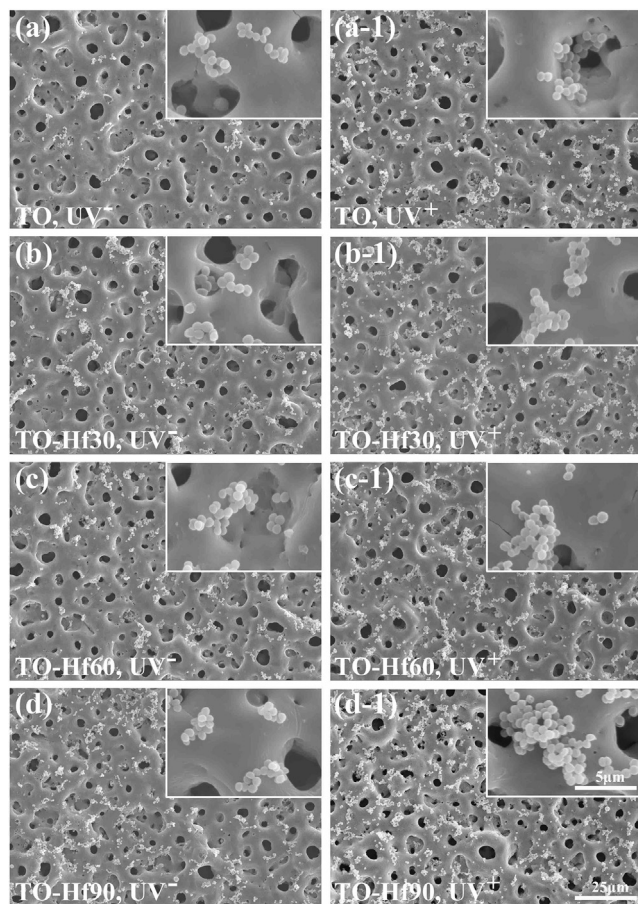


Fig. 7 SEM morphology of the *S. aureus* incubated for 6 h on the samples with (UV⁺) or without (UV⁻) UV pre-treatment: (a) TO, UV⁻, (a-1) TO, UV⁺, (b) TO-Hf30, UV⁻, (b-1) TO-Hf30, UV⁺ (c) TO-Hf60, UV⁻, (c-1) TO-Hf60, UV⁺, (d) TO-Hf90, UV⁻, (d-1) TO-Hf90, UV⁺.

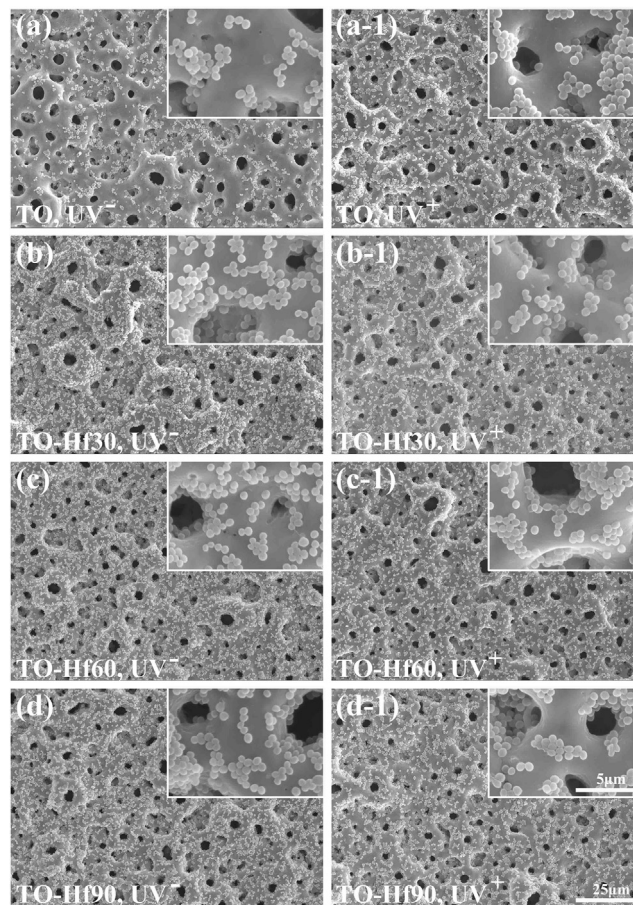


Fig. 8 SEM morphology of the *S. aureus* incubated for 24 h on the samples with (UV⁺) or without (UV⁻) UV pre-treatment: (a) TO, UV⁻, (a-1) TO, UV⁺, (b) TO-Hf30, UV⁻, (b-1) TO-Hf30, UV⁺ (c) TO-Hf60, UV⁻, (c-1) TO-Hf60, UV⁺, (d) TO-Hf90, UV⁻, (d-1) TO-Hf90, UV⁺.

both Hf-doping and UV pre-illumination improved the initial adhesion of bacterial cells on titanium oxide, whereas coupling Hf-PIII treatment and UV pre-illumination had strong activity against microbial adhesion.

3.3. Adhesion of human gingival fibroblasts

The effect of Hf-doping and UV-treatment on the adhesion of Human gingival fibroblasts (HGF) was evaluated by a fluorescent assay. As culturing the cells for 1 h (Fig. 10), the number of adherent cells on the Hf-PIII groups (without UV pre-illumination) was bigger than that on the TO control (the UV-free group); however, the cell spreading areas of the UV-treated groups were smaller than that of their UV-free counterparts, suggesting a negative effect of UV pre-illumination on the initial adhesion (in the first hour) of HGF. As the cell culture duration prolonged to 3 h (Fig. 11), the cell spreading areas of all the sample groups grown larger and the negative effect of UV pre-illumination on adhesion of HGF was gone. These results were consistent with the statistical results shown in Fig. 12. As for culturing of 1 h (Fig. 12a), the cell spreading area of TO, TO-Hf30, TO-Hf60, and TO-Hf90 was 8.63%, 10.95%, 12.77%, and 15.20%, respectively; however, this data for those UV pre-treated groups were only 5.32%, 6.19%, 6.83%, and

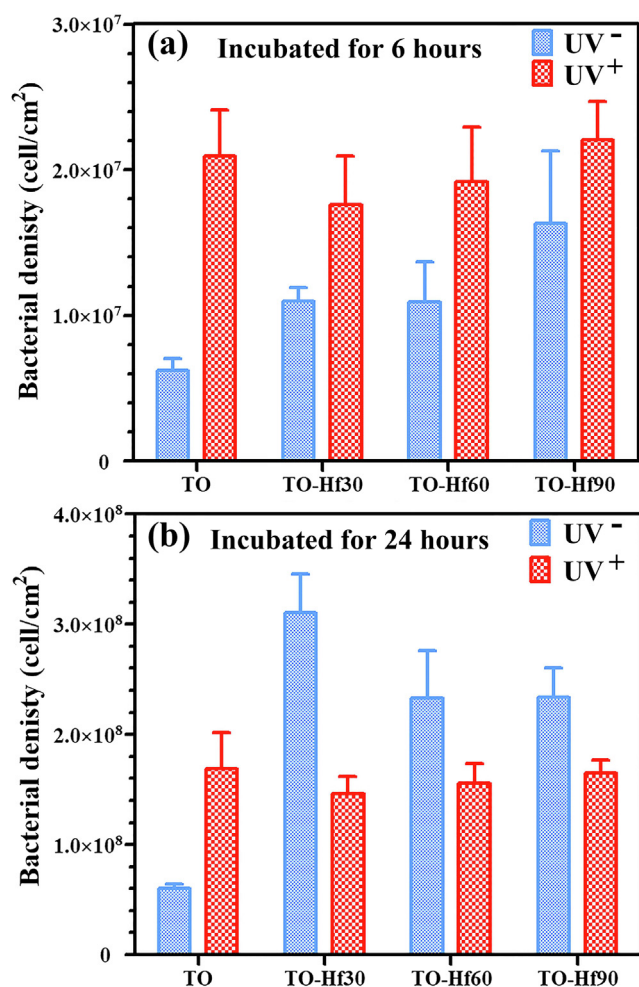


Fig. 9 The corresponding bacterial density on the samples incubated for 6 h (a) and 24 h (b).

9.72%, respectively. As to a 3-hour culture (Fig. 12b), the cell spreading ratio of TO, TO-Hf30, TO-Hf60, and TO-Hf90 was 15.95%, 22.46%, 28.41%, and 35.48%, respectively; and this data for all of the corresponding UV pre-treated groups were 21.02%, 24.87%, 26.77%, and 34.21%, which were about the same level as that on their UV-free counterparts. These data demonstrated that the UV pre-treatment had an adverse effect on the initial adhesion (within the first hour) of HGF cells; however, this negative influence of UV treatment was successfully overcome by the cells within 3 h.

4. Discussion

Cell-selective biomaterials, which favor the attachment of mammalian cells and simultaneously reducing the adhesion of pathogenic microbes, are highly desired in implantable medical devices (Cao et al., 2018, Gristina, 1987, Sanz-Martin et al., 2018). However, due to the same mechanisms shared in attachment by mammalian and bacterial cells (Busscher et al., 2012), it is hard to increase the functions of the former while acting against the latter. Herein, a cell-selectivity, i.e. balanced adhesion of *Staphylococcus aureus* and human gingival fibroblasts, was established on titanium oxide coatings by coupling Hf-PIII treatment and UV pre-illumination, which is

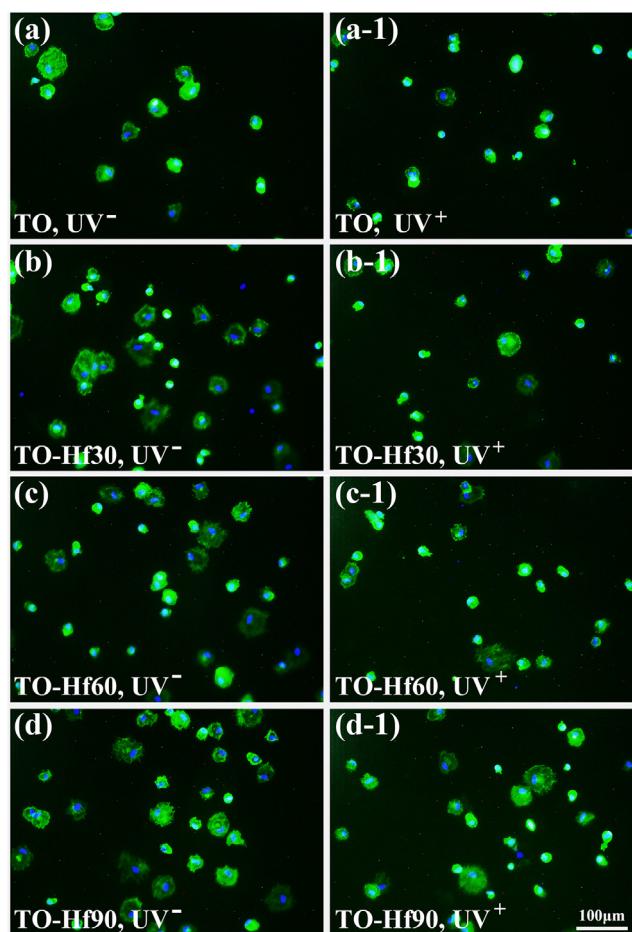


Fig. 10 Fluorescent images of the HGF cultured for 1 h on the samples with (UV⁺) or without (UV⁻) UV pre-irradiation: (a) TO, UV⁻, (a-1) TO, UV⁺, (b) TO-Hf30, UV⁻, (b-1) TO-Hf30, UV⁺, (c) TO-Hf60, UV⁻, (c-1) TO-Hf60, UV⁺, (d) TO-Hf90, UV⁻, (d-1) TO-Hf90, UV⁺. The cell actin stained with FITC (green) and the nucleus stained with DAPI (blue), with a cell density of 2×10^4 cell/mL.

promising for improving the biological performance of titanium-based dental implants.

Inactivating of bacteria by *in situ* light irradiation of titanium oxide during bacterial cultures was reported by many previous studies (Fujishima et al., 2008); however, the exact contribution of UV pre-treatment (the post-illumination effect) on bacterial adhesion is still uncertain. Previously, a bactericidal action of post UV-irradiation was found on the surface of Ti6Al4V (A thin titanium oxide surface layer was likely formed spontaneously due to exposure to the atmosphere) (Gallardo-Moreno et al., 2010); whereas this biocidal activity was not found on UV pre-treated pure titanium (was covered by a thin titanium oxide layer), which merely reduced bacterial adhesion and did not affect the viability of the bacteria (de Avila et al., 2015). In the present study, titanium oxide coatings were produced on pure titanium substrates by using a plasma electrolytic oxidation technique, and some of the titanium oxide coatings were doped with hafnium (Hf) by using a cathodic arc sourced plasma immersion ion implantation & deposition (PIII) technique. As a result, the effects of UV pre-irradiation or/and Hf-doping on *S. aureus* adhesion were

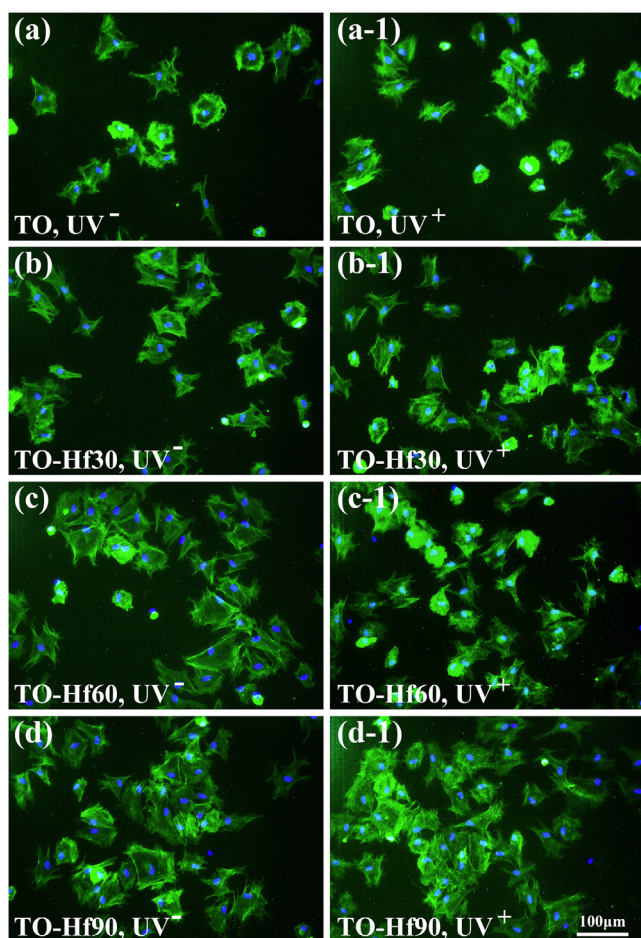


Fig. 11 Fluorescent images of the HGF cultured for 3 h on the samples with (UV⁺) or without (UV⁻) UV pre-irradiation: (a) TO, UV⁻, (a-1) TO, UV⁺, (b) TO-Hf30, UV⁻, (b-1) TO-Hf30, UV⁺, (c) TO-Hf60, UV⁻, (c-1) TO-Hf60, UV⁺, (d) TO-Hf90, UV⁻, (d-1) TO-Hf90, UV⁺. The cell actin stained with FITC (green) and the nucleus stained with DAPI (blue), with a cell density of 2×10^4 cell/mL.

studied. At the early stage of bacterial adhesion (incubated for 6 h, Fig. 9a), the average bacterial density (BD) on the titanium oxide coating was increased due to UV pre-irradiation or/and Hf-doping. However, at the later period (incubated for 24 h, Fig. 9b), the Hf-doped and UV pre-irradiated titanium oxide coatings gained a lower BD than that gained by the groups merely being Hf-doped, indicating a coupling effect of Hf-doping and UV pre-irradiation on bacterial adhesion. Here, the adhesion of bacterial cells could be majorly manipulated by two factors, i.e. the change of wettability due to UV irradiation, and the coupling effect between the doped Hf and the titanium oxide substrate. The water contact angles of the UV positive groups were apparently smaller than their UV negative counterparts. This data indicated that UV pre-irradiation could facilitate bacterial adhesion, which answered for the bigger early stage BD of the UV⁺ groups compared to the UV⁻ counterparts (Fig. 9a). In addition, delayed electron-hole recombination (the decrease of the PL signals, Fig. 5) was detected in the Hf-PIII groups. It was found that the PL signals for hafnium oxide were highly correlated to the concentration of oxygen vacancies in the material (Chuang et al.,

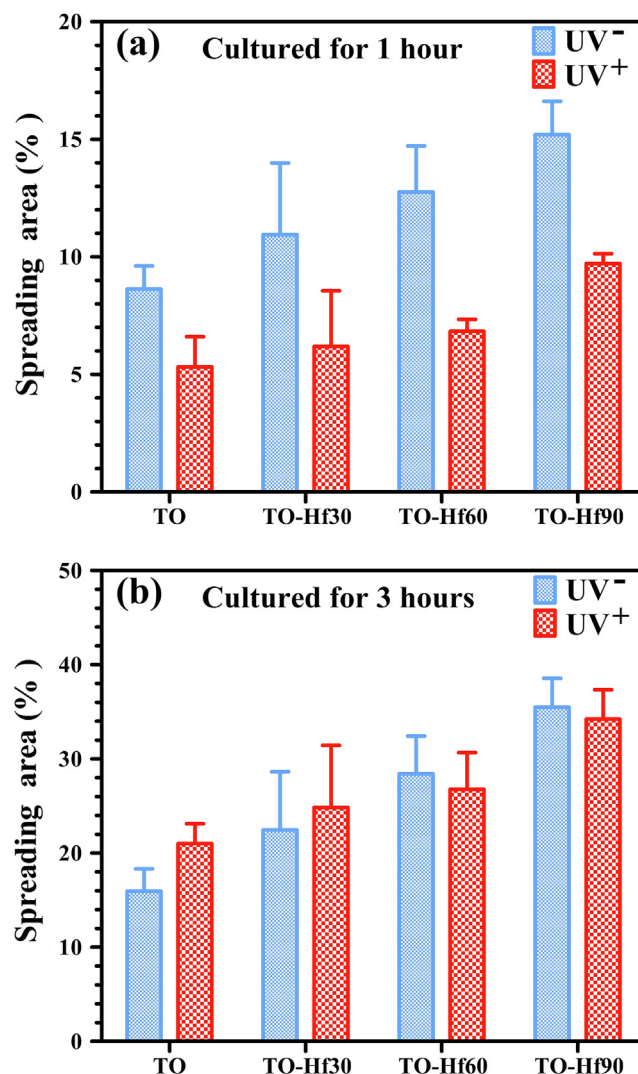


Fig. 12 The corresponding spreading area of the HGF cell cultured for on the samples for 1 h (a) and 3 h (b).

2012), and the oxygen-depleted regions in hafnium oxide or between hafnium and titanium oxide are sensitive to light illumination (Cadieu and Murokh, 2017). Moreover, ion implantation is a nonequilibrium process (Natsuaki et al., 1980), which likely facilitate the generation of oxygen-depleted areas answering for PL signal decreases in the Hf-PIII groups compared to the TO group. Therefore, the prolonged charge separation in the Hf-doped titanium oxide coatings was likely stemmed from the generation of oxygen vacancies in the materials during Hf-PIII. Due to a prolonged electron-hole separation (Fig. 5), the Hf-PIII groups was capable of storing the charges generated by UV pre-illumination, acting against bacterial adhesion. This was consistent with the experimental results on bacterial adhesion (Fig. 9b), which demonstrated that the TO-Hf30, the strongest in delaying charge combination among the Hf-PIII group, gained the biggest decrease (52.9%) compared to its UV negative counterparts. This UV-sensitive coupling behavior between hafnium (Hf) and titanium oxide was also harmful to the initial adhesion of HGF cells (Fig. 12a), but this negative influence was successfully overcome by the cells as the culturing duration prolonged

to 3 h (Fig. 12b), demonstrating a cell-selectivity on hafnium-doped and UV-illuminated titanium oxide coatings.

5. Conclusions

In summary, titanium oxide coatings were produced on pure titanium substrates by using a plasma electrolytic oxidation technique and then doped of hafnium (Hf) by using a cathodic arc sourced plasma immersion ion implantation & deposition (PIII) technique. The Hf-doped titanium oxide coatings had a delayed electron-hole recombination behavior and a UV-illumination dependent charge storage capability, which likely answered for the decreased adhesion of *S. aureus* on UV⁺ and Hf-doped groups. This UV-sensitive coupling behavior between hafnium (Hf) and titanium oxide was also harmful to the initial adhesion of HGF cells, but the negative influence was successfully overcome by the cells as the culturing duration prolonged to 3 h. Taken together, it can be concluded that a cell-selectivity can be established on titanium oxide coating by coupling Hf-doping and UV pre-illumination, which is highly desired in balance the bacterial adhesion and biological sealing of dental implants.

Acknowledgement

This work was jointly supported by grants from the National Natural Science Foundation of China (31670980 and 31870945), the Shanghai Committee of Science and Technology (17441904000), and the Youth Innovation Promotion Association CAS (2015204).

References

- Ananth, H., Kundapur, V., Mohammed, H.S., Anand, M., Amarnath, G.S., Mankar, S., 2015. A review on biomaterials in dental implantology. *Int. J. Biomed. Sci.* 11, 113–120.
- Areid, N., Peltola, A., Kangasniemi, I., Ballo, A., Narhi, T.O., 2018. Effect of ultraviolet light treatment on surface hydrophilicity and human gingival fibroblast response on nanostructured titanium surfaces. *Clin. Exp. Dent. Res.* 4, 78–85.
- Busscher, H.J., Van Der Mei, H.C., Subbiahdoss, G., Jutte, P.C., Van Den Dungen, J., Zaai, S.a.J., Schultz, M.J., Grainger, D.W., 2012. Biomaterial-associated infection: Locating the finish line in the race for the surface. *Sci. Transl. Med.* 4 (10).
- Cadiou, F.J., Murokh, L., 2017. Nanometer thick diffused hafnium and titanium oxide light sensing film structures. *World J. Condens. Matter Phys* 07, 36–45.
- Cao, H., Liu, X., 2013. Activating titanium oxide coatings for orthopedic implants. *Surf. Coat. Technol.* 233, 57–64.
- Cao, H., Qiao, Y., Liu, X., Lu, T., Cui, T., Meng, F., Chu, P.K., 2013. Electron storage mediated dark antibacterial action of bound silver nanoparticles: Smaller is not always better. *Acta Biomater.* 9, 5100–5110.
- Cao, H., Qiao, Y., Meng, F., Liu, X., 2014. Spacing-dependent antimicrobial efficacy of immobilized silver nanoparticles. *J. Phys. Chem. Lett.* 5, 743–748.
- Cao, H.L., Tang, K.W., Liu, X.Y., 2018. Bifunctional galvanics mediated selective toxicity on titanium. *Mater. Horiz.* 5, 264–267.
- Chuang, S.-H., Lin, H.-C., Chen, C.-H., 2012. Oxygen vacancy relationship to photoluminescence and heat treatment methods in hafnium oxide powders. *J. Alloys Compd.* 534, 42–46.
- De Avila, E.D., Lima, B.P., Sekiya, T., Torii, Y., Ogawa, T., Shi, W., Lux, R., 2015. Effect of UV-photofunctionalization on oral bacterial attachment and biofilm formation to titanium implant material. *Biomaterials* 67, 84–92.
- Derks, J., Tomasi, C., 2015. Peri-implant health and disease. A systematic review of current epidemiology. *J. Clin. Periodontol.* 42, S158–S171.
- Domaradzki, J., Kaczmarek, D., Prociow, E.L., Borkowska, A., Kudrawiec, R., Misiewicz, J., Schmeisser, D., Beuckert, G., 2006. Characterization of nanocrystalline TiO₂-HfO₂ thin films prepared by low pressure hot target reactive magnetron sputtering. *Surf. Coat. Technol.* 200, 6283–6287.
- Fujishima, A., Zhang, X.T., Tryk, D.A., 2008. TiO₂ photocatalysis and related surface phenomena. *Surf. Sci. Rep.* 63, 515–582.
- Gallardo-Moreno, A.M., Pacha-Olivenza, M.A., Fernandez-Calderon, M.-C., Perez-Giraldo, C., Bruque, J.M., Gonzalez-Martin, M.-L., 2010. Bactericidal behaviour of Ti6Al4V surfaces after exposure to UV-C light. *Biomaterials* 31, 5159–5168.
- Glazer, P.M., Sarkar, S.N., Summers, W.C., 1986. Detection and analysis of UV-induced mutations in mammalian-cell DNA using a lambda-phage shuttle vector. *Proc. Natl. Acad. Sci. U. S. A.* 83, 1041–1044.
- Gristina, A.G., 1987. Biomaterial-centered infection - microbial adhesion versus tissue integration. *Science* 237, 1588–1595.
- Iwasa, F., Hori, N., Ueno, T., Minamikawa, H., Yamada, M., Ogawa, T., 2010. Enhancement of osteoblast adhesion to UV-photofunctionalized titanium via an electrostatic mechanism. *Biomaterials* 31, 2717–2727.
- Miyauchi, T., Yamada, M., Yamamoto, A., Iwasa, F., Suzawa, T., Kamijo, R., Baba, K., Ogawa, T., 2010. The enhanced characteristics of osteoblast adhesion to photofunctionalized nanoscale TiO₂ layers on biomaterials surfaces. *Biomaterials* 31, 3827–3839.
- Nakano, R., Ishiguro, H., Yao, Y.Y., Kajioaka, J., Fujishima, A., Sunada, K., Minoshima, M., Hashimoto, K., Kubota, Y., 2012. Photocatalytic inactivation of influenza virus by titanium dioxide thin film. *Photochem. Photobiol. Sci.* 11, 1293–1298.
- Natsuaki, N., Tamura, M., Tokuyama, T., 1980. Non-equilibrium solid-solutions obtained by heavy-ion implantation and laser annealing. *J. Appl. Phys.* 51, 3373–3382.
- Renvert, S., Persson, G.R., Piri, F.Q., Camargo, P.M., 2018. Peri-implant health, peri-implant mucositis, and peri-implantitis: Case definitions and diagnostic considerations. *J. Periodontol.* 89, S304–S312.
- Sanz-Martin, I., Sanz-Sanchez, I., De Albornoz, A.C., Figuero, E., Sanz, M., 2018. Effects of modified abutment characteristics on peri-implant soft tissue health: A systematic review and meta-analysis. *Clin. Oral Implants Res.* 29, 118–129.
- Visai, L., De Nardo, L., Punta, C., Melone, L., Cigada, A., Imbriani, M., Arciola, C.R., 2011. Titanium oxide antibacterial surfaces in biomedical devices. *Int. J. Artif. Organs* 34, 929–946.
- Wang, Y.J., Lin, Z.L., Cheng, X.L., Xiao, H.B., Zhang, F., Zou, S.C., 2004. Study of HfO₂ thin films prepared by electron beam evaporation. *Appl. Surf. Sci.* 228, 93–99.
- Williams, D.F., 2008. On the mechanisms of biocompatibility. *Biomaterials* 29, 2941–2953.
- Yadav, A., Yadav, R., Gupta, A., Baranwal, A., Bhatnagar, A., Singh, V., 2017. Effect of ultraviolet irradiation on the osseointegration of a titanium alloy with bone. *Contemp. Clin. Dent.* 8, 571–578.
- Zhang, J., Wang, H.M., Wang, Y., Dong, W.J., Jiang, Z.W., Yang, G. L., 2018. Substrate-mediated gene transduction of lama3 for promoting biological sealing between titanium surface and gingival epithelium. *Colloids Surf., B* 161, 314–323.